文章编号：1001－9014(2019)05－0572－06

DOI:10.11972/j.issn.1001－9014.2019.05.005

Investigation of large power microwave nonlinear effects on amplitude-phase controller chip for Ka-band phased array radar T/R modules

GUO Guo[1*], XU Xiong[2], WEI Yan-Yu[1], GUO Chang-Yong[3]

(1. School of Electronic Science and Engineering, University of Electronic Science and Technology of China, Chengdu 610054, China;
2. State Key Laboratory of Complex Electromagnetic Environment Effects on Electronics and Information System (CEMEE), Luoyang 471003, China;
3. Department of mechanical and electrical engineering, Nanyang Technician College, Nanyang 473000, China)

Abstract: Large power microwave nonlinear effects on amplitude-phase controller chip were experimentally tested and theoretical analyzed. This chip had the typical application on Ka-band phased array radar (PAR) transmit/receive (T/R) modules. The test platform was built up by a solid source and a pulsed magnetron to generate large power Ka-band microwave. The degradation and destroy phenomenon were observed distinctly as the input power amplitudes were improved. The total-state phase characteristics and the degradation thresholds of the selected chip are obtained through a series of experimental tests. At last, the results are given by figures and the damage mechanism is theoretically analyzed.

Key words: radio physics, nonlinear effects, experimental test, amplitude-phase controller chip, T/R modules, large power microwave

PACS: 07.57.-c, 85.30.-z, 84.40.Xb, 41.20.-q

Ka波段相控阵雷达TR组件幅相控制芯片的大功率微波非线性效应研究

郭 骥[1*], 许 雄[2], 魏彦玉[1], 郭长永[3]

(1. 电子科学与工程学院,电子科技大学,四川 成都 610054;
2. 电子信息系统复杂电磁环境效应国家重点实验室,河南 洛阳 471003;
3. 南阳技师学院,河南 南阳 473000)

摘要:采用实验测试和理论分析的方法研究了幅相控制芯片的大功率微波非线性效应.该芯片应用于Ka波段相控阵雷达收发组件中.测试平台利用固态源和脉冲磁控管来产生Ka波段大功率微波.随着输入功率幅值的提高,在实验中很明显地观测到了芯片的降级和毁伤现象.通过一系列的实验测试得到了芯片的全态相移特性和降级阈值,并通过图片给出了实验结果.最后,通过理论分析给出了该芯片的毁伤机理.

关 键 词:无线电物理学;非线性效应;实验测试;幅相控制芯片;T/R组件;大功率微波

中图分类号:TN62　　**文献标识码**:A

Introduction

In recent years, the operational capabilities of phased array radar, especially the modern active digital-controlled phased array radar (PAR), offers previously unknown advantages to users[1-3]. In modern radar system, transmit/receive (T/R) modules occupy about 70% percent weights of the PAR antenna[4-5]. T/R modules are comprised of semiconductor devices and chips, which are always the typical "front door" attacking target of the high power microwave (HPM)[6-7]. For most cases, the large power microwave signals are coupled through a receiving antenna to cause the degradation and

Received date: 2018-08-11, **revised date**: 2018-11-19　　**收稿日期**:2018-08-11, **修回日期**:2018-11-19

Foundation items: Supported by the Fundamental Research Funds for the Central Universities (ZYGX2018J032), the National Natural Science Foundation of China (61571078, 61801088, 11505043) and the National Key R&D Program of China (2017YFE0300200, 2017YFE0300201)

Biography: GUO Guo (1985-), male, Hehan, Docter, assistant researcher. Research area involves millimeter system and vacuum electron devices. E-mail: guoguouestc@126.com

* **Corresponding author**: E-mail: guoguouestc@126.com

damage of the chips and the systems. As a critical part in T/R modules, once the amplitude-phase controller chip is attacked, the phase scanning function in any direction of the PAR in the digital domain could be lost. So the reliability and the input power capacity of the T/R modules always determine the performance of the whole radar system.

As the most important components in the amplitude-phase controller chip, phase shifters have lots of types according to different operational principles[8-9]. Of all types, ferrite phase shifters and semiconductor phase shifters are potential candidates applied in T/R modules. Ferrite phase shifters are slow to respond to control signals and difficult to be used in rapid beam scanning. Although with the disadvantages of relative higher losses at microwave and millimeter-wave frequencies, semiconductor device phase shifters have much faster response speeds. As a result, semiconductor phase shifter integrated in the amplitude-phase controller chip is widely used in modern PAR systems[8].

However, the major drawback with semiconductor phase shifters is that they have limited power-handling capability. So it is necessary to investigate the linear and nonlinear power effects of the amplitude-phase controller chips under the HPM irradiation. Unfortunately, rare researches on this field have been reported until now.

In this paper, we focus on this problem and select a chip of amplitude-phase controller as the experimental target of the large microwave power. At first, the test fixtures are designed and assembled with the chip according to the chip structure in the datasheet. After that, the low power linear characteristics of the chip are tested by a fixed-output continuous wave (CW) source. Moreover, the large power nonlinear characteristics are investigated by the high power pulsed magnetron. The degradation thresholds and mechanism are analyzed theoretically finally.

1　Test platform and system

Amplitude-phase controller components and their positions in the T/R module are shown in Fig. 1. In modern T/R module, the RF switch, the phase shifter, and the attenuator are always designed together as a chip of amplitude-phase controller. The amplitude-phase controller chip is always located behind the amplifier along the receiving branch in the whole system.

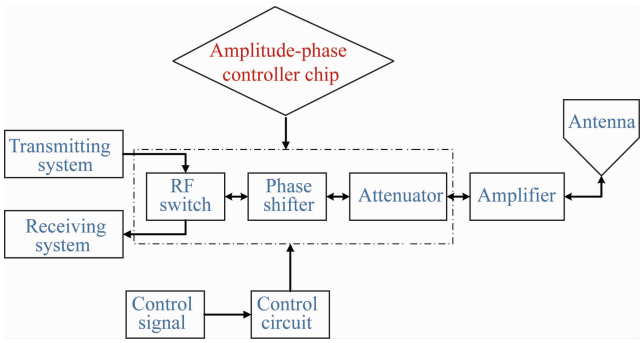

Fig. 1　Amplitude and phase controller components of the T/R module

图 1　T/R 组件中的幅度和相位控制器件

Based on the structure analysis of the T/R module, we select one type of the amplitude-phase controller chip as the experimental target because it is the significant control core in the whole system. According to the critical parameters in the datasheet of the selected chip shown in Table 1, test fixtures are designed and fabricated for the matching and connections from the chips to the outside circuit by using the gold wire-bounding. Fig. 2 gives the sketch of the fixture, together with the assembled amplitude-phase controller chip.

Table 1　Critical parameters of the selected amplitude-phase controller chip in its datasheet

表 1　幅相控制芯片数据表中的关键参数

Operation frequency/GHz	34 ~ 36
Operation voltage/V	-5/5
Insertion loss of the full-state/dB	10
phase shifter bit	6
phase shifter stepping/degrees	5.625
phase shifter precision/degrees	2
phase shifter range/degrees	0 ~ 360

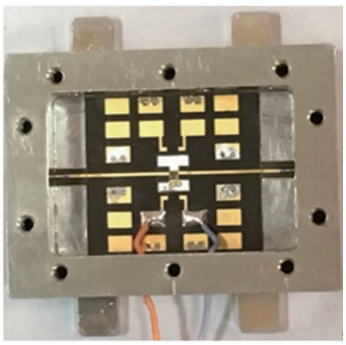

Fig. 2　Sketches of the chip dimensions and the test fixture for the amplitude-phase controller chip

图 2　幅相控制芯片的尺寸和测试夹具示意图

Test platform is comprised of more than ten components, which is shown in Fig. 3. The whole system is built on the basis of the signal coupling path from the microwave source to the targets. A large power signal is generated from the source through the 20dB adapted attenuator, and transmitted by a rectangular horn antenna. Then the signal is received by another rectangular horn antenna and sampled by a 10dB directional coupler. After a 90° curved waveguide, the signal is attenuated by a fixed attenuator. Two pairs of converters including waveguide-coaxial converters and coaxial-SMP converters are used to achieve matching between the test fixture and the outside circuit. At last, the output signal is detected by the detector and analyzed by the equipment.

In the test platform above, a Ka-band solid-state CW source with fixed output power and a Ka-band high power pulsed magnetron are employed as microwave sources. The output power of the Ka-band solid-state CW source is fixed on about 1W and the frequency can be adjusted from 34 GHz to 36 GHz. The power level of the pulsed magnetron is above a kilowatt and we can adjust

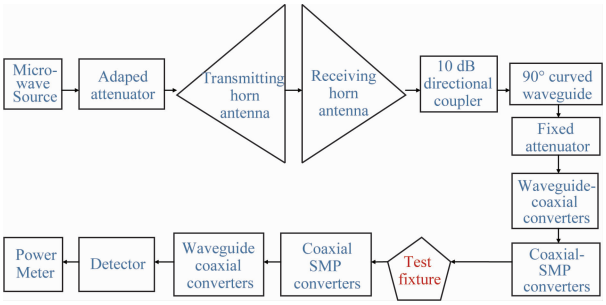

Fig. 3 Test platform and each component
图3 测试平台和各部件

the power amplitude by different attenuators. The whole system also includes other assistant equipment, such as power supply, radiator and so on.

2 Experimental test processes

At the beginning of the experiments, the initial phase shifting characteristics of the chip are tested by the vector network analyzer (VNA). At 34.9GHz, the initial phase state is tested and shown in the Fig. 4 (a). For comparison, half phase shift state (180 degrees) of this chip from the VNA is shown in Fig. 4 (b). We can see that the initial phase state is −41.4 degrees and the half phase shift state is 146.4 degrees after 180-degree phase shifting, which indicates that the phase shift function of the amplitude-phase controller chip is normal and the phase shift precision is acceptable according to the data shown in Table. Ⅰ. The S_{21} parameters in the frequency band of 34 GHz to 36 GHz are around −10 dB, which illustrates the total insertion losses of the chip are normal. Comparisons of the phase and the S_{21} parameters between the two states above are draw in Fig. 4(c) and Fig. 4(d), respectively.

Our tests are divided into two steps as below, including the CW lower power test and the pulsed larger power test:

In the first experimental stage, the solid-state CW source is used to test the lower power level (below 25 dBm) characteristics of the chip. For the maximum output power of the solid-state CW source is 30 dBm, the maximum power injected to the chip is about 25 dBm besides all insertion losses of the test platform. To investigate the gain property more accurately, the input power is measure every time. The input power can be obtained directly as the power meter indication at the end of the system.

In the large power (above 25 dBm) test, a magnetron is employed to generate several kilowatts pulsed signal. For the pulsed power level is far beyond the capacity of the power meter, a detector and an oscilloscope are needed to calibrate the microwave power. Before that, a power calibration for the detector is necessary to build up the relationship between the voltage levels revealed in the oscilloscope and the accurate power amplitude of the pulsed signal, which is shown in Fig. 5. After each test, the fixture is taken down from the test platform and off-line test for the phase shifting performance is carried out

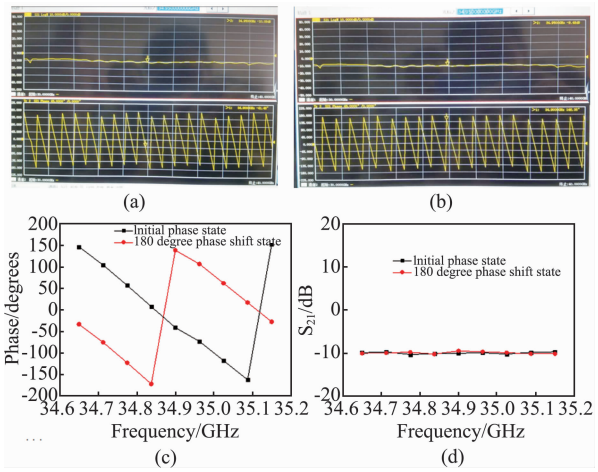

Fig. 4 Initial phase state (a) and the half phase shift state (180 degrees), (b) shown in the VNA and the comparisons of the phase, (c) and the S_{21} parameters, (d) between the two states before test
图4 实验前矢网显示初始状态(a),半全态移相状态(180度)(b),两种状态相位的对比(c)和两种状态 S_{21} 参数的对比(d)

by using a VNA. The off-line test method could protect the expensive VNA from the large power signal irradiation. By repeating the process above for several times as the improvement of the input power and comparing the phase shift capacity before and after receiving the large power signal, the linear and nonlinear characteristics of the chip can be obtained.

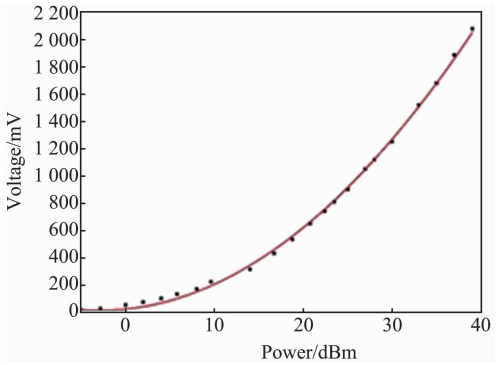

Fig. 5 Power calibration for the detector before test
图5 实验前对检波器的功率标定

3 Test results

As the most significant parameters of the amplitude-phase controller chip, the phase shifting capacity and the insertion loss can directly reflect the performance and the damage level. Both two parameters can be investigated by the VNA. Results from the two-step test are as follows:

① CW input power is improved starting from −15 dBm per 1dBm and the off-line test results are observed for every irradiation. When the CW signal from the solid-

state source reaches the upper limitation 30 dBm, the phase shifting capacity and the insertion loss shown in the VNA are still normal.

② Large power pulsed signals generated from the magnetron are employed in the following test. The phase shift capability of the chip keeps normal until the input voltage level reaches 1.25 V in the oscilloscope, which is shown in Fig. 6 (a). The typical data can be extracted and drawn as Fig. 6 (b). The pulse width of the signal is 168.4 ns. According to the power calibration between the voltage level and the accurate power amplitude shown in Fig. 5, this input power amplitude is 31 dBm. Fig. 7 gives the off-line test results from the VNA after one pulse irradiation.

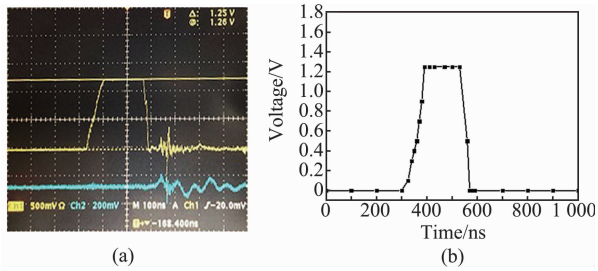

Fig. 6　Microwave signals displayed in the oscilloscope (a) and extracted pulsed wave profile (b)
图 6　示波器上的微波信号显示(a)和提取的脉冲波形(b)

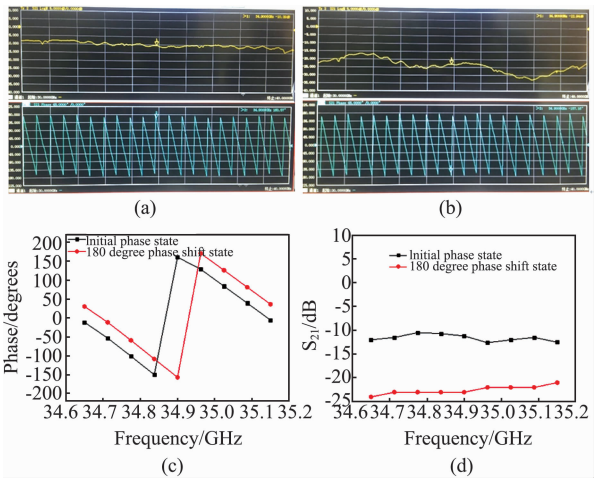

Fig. 7　Initial phase state (a) and the half phase shift state (180 degree) (b) shown in the VNA after 31 dBm pulsed signal irradiation and the comparisons of the phase (c) and the S_{21} parameters (d) between the two states after test
图 7　31 dBm 脉冲信号辐照后示波器上显示的初始相位(a),半全态相位(180 度)(b),两种状态相位的对比(c)和两种状态 S_{21} 参数的对比 (d)

Compared to the initial phase shifting characteristics shown in Fig. 4, three abnormal phenomena suddenly appear from the off-line test results:

① The initial phase state changes from −41.4 degrees to 160.5 degrees.

② Secondly, the initial phase state is 160.5 degrees and the half phase shift state is −157.1 degrees after 180-degree phase shifting. Totally, the difference between these two state is only 42.4 degrees.

③ Thirdly, the insertion loss of the half phase shift state increases sharply from 9.48 dB to 22.94 dB.

Based on the performance comparison results between the first test and the last test, we can make the conclusion that the chip has been degraded after irradiated by the large power signal with the threshold of 31dBm. At last, the comparisons for typical parameters of the chip before and after the experiments are summarized in Table 2, in which the destroy points under the microscope after the experiments are shown in Fig. 10 (b).

Table 2　Parameters of the chip comparison before and after the experiments
表 2　实验前后芯片参数的对比

	Initial test	Test after the experiments
Ground-state phase/degrees	−41.4	160.5
Phase shifting capacity/degrees	187.8	42.4
Insertion loss of the half phase shift state/dB	9.48	22.94
Destroy points under the microscope	None	Have
Status	Normal	Unrecoverable damage

4　Damage mechanism analysis

On the device level, the phase shifter can be simplified as a two-port network that provides the phase difference between output and input signals, which is shown in the Fig. 8. The two single pole double throw switch (SPDT) is used to control the signal path with the reference phase Φ1. When the input signal switches from the network 1 to the network 2, the phase difference (Φ2 − Φ1) shift can be achieved.

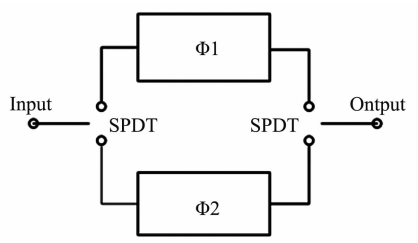

Fig. 8　Basic structure of phase shifter
图 8　移相器的基本结构

The six-bit digital phase shifters are cascaded by 5.625°, 11.25°, 22.5°, 45°, 90°, and 180° phase shifter units, as shown in Fig. 9. Different conditions of shift phase between 0-360° with the step of 5.625° are controlled by series of digital signals generated from a data control board. From the total-state phase shift characteristics, it can be seen that each digital phase shifter in the amplitude-phase control chip has been damaged because of the most uniform phase difference between neighboring two states.

On the semiconductor structure level, RF switches in the amplitude-phase control chip are consist of GaAs

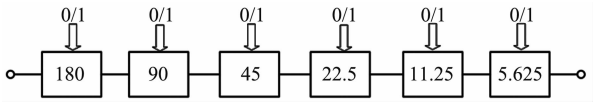

Fig. 9 System block diagram of a six-bit digital phase shifter, in which the unit of the shift phases are degrees
图 9 六位移相器的系统框图,图中的相移量单位为度

PIN diodes. GaAs pin diodes have advantages of low conductivity, small knot capacitance and easy integration to make the RF switches with the small insertion loss, wide bandwidth and small size. The damage mechanism of the large power microwave of the amplitude-phase control chip is mainly the breakdown effect of the pin diode after the irradiation of the large power microwave pulse shown in Fig. 10 (a). This is approved by the amplitude-phase control chip photograph observed by microscope in Fig. 10 (b). As shown, the phase shifter consists of transmission lines, delay lines and PIN diodes. Two obvious destroy points appear on the photograph.

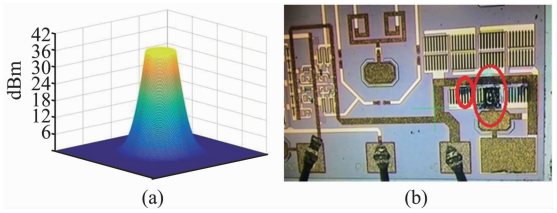

Fig. 10 Chip photograph under the microscope (b) after large power signal irradiation (a)
图 10 大功率微波信号的三维电磁场强度分布图(a)及被辐照后显微镜下的芯片(b)

The structure of the GaAs PIN diode, as shown in Fig. 11, is inserted by an unbound intrinsic layer (I layer) between the P-type semiconductor and the N-type semiconductor to form a vertical structure pin diode. In forward bias, pin diode has a small conduction resistance. When the reverse bias is applied, the diode's conduction resistance becomes very large and the junction capacitance are approximate to a constant value.

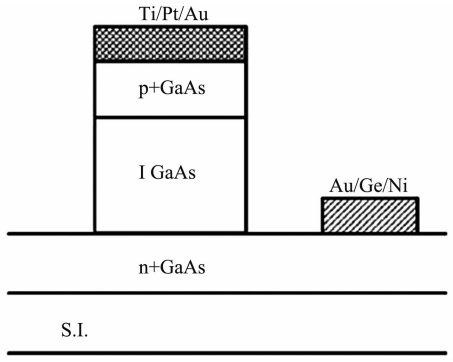

Fig. 11 Structure of GaAs PIN diodes
图 11 砷化镓(GaAs)PIN 二极管的结构

For the sub-microsecond (100 ns ~ 1μs) pulse width, the damage mechanism of the PIN diodes in this paper can be explained with the theory of the current filaments [10-11]. According to this theory, the formation of current filament is caused by the negative resistance effect after the avalanche breakdown of PIN diode. Due to the self-heating effect of current filament and the negative temperature coefficient of the avalanche ionization rate, the current filament moves back and forth in the PIN diode. When the irradiation power reaches a certain value (the threshold of 31dBm), the thermal excitations replace the avalanche excitations as the main source of the carrier, and the avalanche current filament is changed into the thermoelectric filament. The heat production rate has a positive temperature coefficient, so the higher of the heat production rate in the region of the high temperature, the higher of the carrier concentration and the higher of the current density and the power consumption. Thus the further raising of the temperature forms a thermoelectric positive feedback. The thermoelectric filament is fixed to the edge of the device by this positive feedback mechanism and shrinks continuously, while the center temperature rises rapidly leading to the damage of the PIN diode eventually.

5 Conclusion and discussion

The amplitude-phase controller chip for Ka-band T/R module of PAR is selected as large power signal targets. After fabrication of the test fixture and building up of the test platform, the irradiation experimental tests are carried out. For the amplitude-phase controller chip, a single pulse with the power amplitude of 31 dBm can lead to the unrecoverable damage and phase shift function loss. Besides, the initial phase state is changed and the insertion loss of the half phase shift state increases sharply. We believe that these experimental results can provide significant references for the large power signal and the PAR researches in the future.

There are still some practical issues that need to be discussed. First, the accuracy of power calibration for the detector is critical for our test, so we would calibrate the detector as accurate as possible and try different detectors. Second, more chips for the same or different batches should be employed to eliminate system errors in order to obtain more typical results.

References

[1] Salvador H. Talisa, Kenneth W. O'Haver, Thomas M. Comberiate, *et al.* Somerlock. Benefits of Digital PARs [C], Proceedings of the IEEE, **104**(3), March 2016.

[2] Ryszard Bil, Wolfgang Holpp, Electronics and Border Security, Modern PAR Systems in Germany [C], Phased Array Systems and Technology (PAST), IEEE International Symposium on, Waltham, MA, USA, 2016.

[3] Judson E. Stailey, Kurt D. Hondl, Multifunction PAR for Aircraft and Weather Surveillance [C], Proceedings of the IEEE, **104**(3), March 2016.

[4] T. R. Turlington, F. E. Sacks, J. W. Gipprich, T/R Module Architectural Consideration for Active Electronically Steerable Arrays[C]. IEEE MTT-S Digest, 1992.

[5] Adrian Garrod, Digital Modules for Phased Array Radar [C], *IEEE International Radar Conference*, 1995.

[6] D Massé, Lockheed Martin Awarded High-power Microwave Energy Weapon Contract [J], *Microwave Journal*, 2013, **53**(12) :41-41.

[7] Guo Guo, Ling Gu, Ruowu Wu, *et al.* Large power microwave nonlin-

ear effects on multifunction amplifier chip for Ka-band T/R module of phased array radar [J], *Aip Advances*, 2017, **7**(125226): 125226-1-125226-11.

[8] Erich G. Erker, Amit S. Nagra, Yu Liu, *et al.* Taylor, James Speck, and Robert A. York, Monolithic Ka-Band Phase Shifter Using Voltage Tunable BaSrTiO3 Parallel Plate Capacitors [J], *IEEE Microwave And Guided Wave Letters*, 2000, **10**(1): 10-12.

[9] Franco De Flaviis, N. G. Alexopoulos, and Oscar M. Stafsudd. Planar Microwave Integrated Phase-Shifter Design with High Purity Ferroelectric Material [J], *IEEE Transactions On Microwave Theory And Techniques*, June, 1997, **45**(6): 963-969.

[10] Ren Xingrong, Chai Changchun, Ma Zhenyang, *et al.* Motion of current filaments in avalanching PIN diodes[J], *Journal of Semiconductors*, April, 2013, **34**(4): 37-41.

[11] Xingrong Ren, Research on the Electromagnetic Damage Effects and Mechanisms of Semiconductor Devices [D]. Xi'an: Xidian University, (任兴荣,半导体器件的电磁损伤效应与机理研究. 西安:西安电子科技大学), 2014.